Yoshiki Yoshida
Associate Professor.
e-mail: yoshida@me.es.osaka-u.ac.jp

Yoshinobu Tsujimoto
Professor.

Graduate School of Engineering Science,
Osaka University,
1-3, Machikaneyama, Toyonaka,
Osaka 560-8531, Japan

Nobuhiro Ishii
Engineer, Hitachi Construction
Machinery Co., Ltd.,
650, Kandatsu, Tsuchiura,
Ibaraki 300-0012, Japan

Hideo Ohashi
President, Kougakuin University,
1-24-2, Nishishijuku Shinjuku,
Tokyo 163-8677, Japan

Fumitaka Kano
Professor, Nara National
College of Technology,
22, Yata, Yamatokoriyama,
Nara 639-1058, Japan

The Rotordynamic Forces on an Open-Type Centrifugal Compressor Impeller in Whirling Motion

In recent years, increasing interest has been given to the rotordynamic forces on impellers, from the view point of the shaft vibration analysis. Previous experimental and analytical results have shown that the fluid-induced forces on closed-type (with shroud) centrifugal impellers in whirling motion contribute substantially to the potential destabilization of subsynchronous shaft vibrations. However, to date nothing is known of the rotordynamic forces on open-type (without shroud) centrifugal impellers. This paper examines the rotordynamic fluid forces on an open-type centrifugal compressor impeller in whirling motion. For an open-type impeller, the variation of the tip clearance due to the whirling motion is the main contribute to the rotordynamic forces. Experiments were performed to investigate the rotordynamic forces by direct measurement using a force balance device, and indirectly from the unsteady pressure on the casing wall over a range of whirl speed ratio (Ω/ω) for several flow rates. In this paper, the following results were obtained: (1) Destabilizing forces occur at small positive whirl speed ratio ($0 < \Omega/\omega < 0.3$) throughout the flow range of normal operation; (2) At smaller flow rate with inlet backflow, the magnitude of the fluid force changes dramatically at a whirl speed ratio close to $\Omega/\omega = 0.8$, resulting in destabilizing rotordynamic forces. From the measurement of unsteady inlet pressure, it was shown that the drastic changes in the fluid force are related to the coupling of the whirling motion with a rotating flow instability, similar to "rotating stall"; (3) The forces estimated from the unsteady pressure distribution on the casing wall and those estimated from the pressure difference across the impeller blades were compared with the results from the direct fluid force measurements. The direct fluid forces correlate better with the forces due to the pressure distribution on the casing wall.

Introduction

Over the last ten years many experimental and analytical data have been obtained on the fluid-induced rotordynamic forces on pump impellers, mainly at Caltech and the University of Tokyo. It is now widely recognized that for closed-type (with shroud) centrifugal impellers, the fluid forces become destabilizing for the forward whirl generally at whirl speed ratio (Ω/ω) less than 0.5 (Jery et al., 1985; Bolleter et al., 1987; Ohashi et al., 1988). The destabilizing forces are caused by the unsteady interaction between the impeller and volute casing (Adkins et al., 1988; Tsujimoto et al., 1988a) or vaned diffuser (Tsujimoto et al., 1988b), or by unsteady leakage flow that surrounds the impeller shroud (Childs, 1989; Guinzburg et al., 1994). All these works have been summarized in the recent textbooks of Childs (1993) and Brennen (1994), which are extremely helpful and useful for shaft vibration analysts.

For axial turbomachines, the destabilizing mechanism associated with the tip clearance flow was first postulated by Thomas (1958) and Alford (1965). Their model explaining the destabilizing tangential force has been widely accepted. They pointed out that: in a turbine operating with an eccentric rotor, blades with smaller tip clearance would produce greater circumferential driving force than blades at the diametrically opposite position with larger tip clearance. This difference in blade loading results in a tangential force promoting the forward whirl. Recently, for axial compressors operating with rotor eccentricity, it was reported that the destabilizing whirl direction depends on the flow rate (Colding-Jorgensen, 1992; Ehrich, 1993). In addition, an MIT group investigated the rotordynamic forces on the axial flow turbine for the SSME (Space Shuttle Main Engine), both experimentally (Martinez-Sanchez et al., 1995) and analytically (Song et al., 1997). They reported that the fluid force on the rotor is basically generated as a result of the nonuniform blade loading, as explained by Thomas and Alford, with some fraction of the force caused by the nonuniform pressure distribution around the rotor.

Open-type impellers have been widely used for high-speed and high-pressure centrifugal compressors. Nevertheless, as far as the authors are aware, no rotordynamic data for these machines are available. This paper presents the results from an investigation of the rotordynamic fluid forces on an open-type centrifugal compressor impeller. Fluid forces were measured directly with a force balance device. Discussions on the unsteady pressure measurements on the casing wall, and blade to blade pressure distributions are also presented.

Experimental Facility

Description of Test Facility. Figure 1 shows the mechanism to generate the whirling motion. The inner sleeve supports the main shaft through two eccentric inner bearings set to produce a pure whirling motion. The main shaft is driven by an AC motor with the rotational speed (ω) through the universal joint, and the outer sleeve is driven by a DC motor controlled to run at a prescribed whirling speed (Ω). The main shaft speed was maintained at 400 ± 1 rpm, and the whirl speed ratio (Ω/ω) was varied in the range from -1.4 to $+1.4$. Uncertainty in the whirl speed

---

Contributed by the Fluids Engineering Division for publication in the JOURNAL OF FLUIDS ENGINEERING. Manuscript received by the Fluids Engineering Division August 17, 1998; revised manuscript received March 15, 1999. Associate Technical Editor: B. Schiavello.

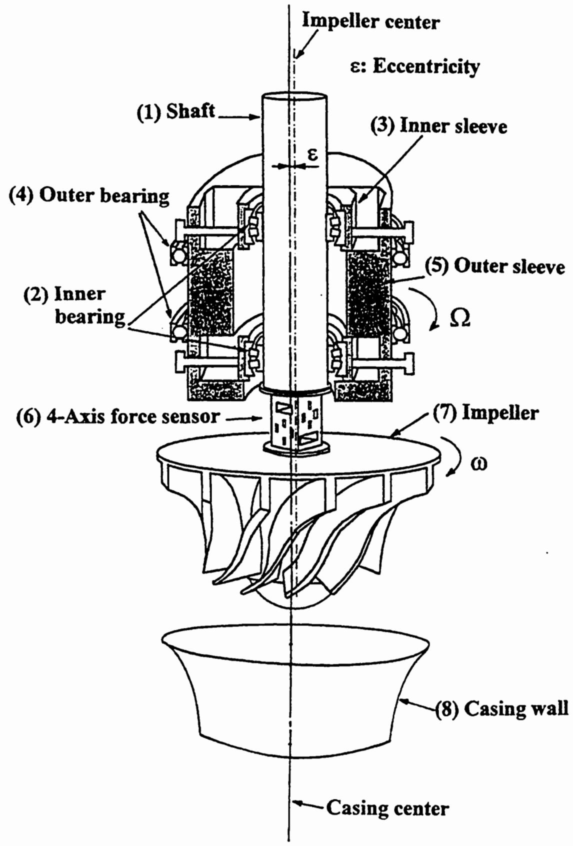

Fig. 1 Mechanism to produce the impeller whirling motion

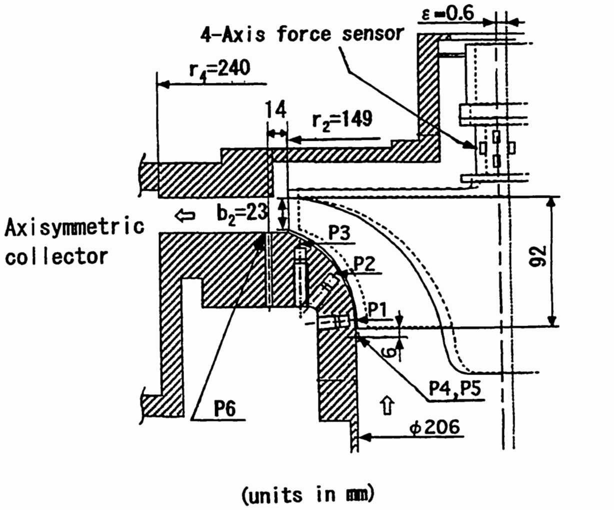

Fig. 2 Cross section of the test rig (impeller, casing and instrumended shaft)

ratio, Ω/ω, is ±0.002. A detailed description of the facility can be found in Ohashi et al. (1991).

Figure 2 shows the details around the impeller. The test impeller is a model of an industrial centrifugal compressor with 12 blades (Z_i), inlet blade angle 32 deg and outlet 45 deg at the tip (i.e., back swept blade), outer radius (r_2) 149 mm, exit width (b_2) 23 mm; its nondimensional type number is 1.3. The impeller was running inside a vaneless diffuser with radius ratio $r_4/r_2 = 1.61$ and a symmetrical collector to minimize the interaction with stationary parts. Although the test impeller was designed for gas, water was used as the working fluid to facilitate the measurement of the fluid forces. The Reynolds number ($\mathrm{Re} = u_2 r_2/\nu$, $u_2 = r_2\omega$) is 3.0~4.0 × 10^6 for actual condition (air, u_2 = 300~400 m/s), and 0.92 × 10^6 for this laboratory test condition (water, u_2 = 6.2 m/s). The effect of compressibility of actual working fluid (gas) is neglected in the test condition (water). Under the condition without eccentricity, the blade tip normal clearance is constant (1 mm)

Nomenclature

b_2 = impeller axial width at outlet = 23 mm (see Fig. 2)
C = dimensionless direct damping coefficient, normalized by $\rho\pi r_2^2 b_2\omega$
c = dimensionless cross-coupled damping coefficient, normalized by $\rho\pi r_2^2 b_2\omega$
ΔC_p = coefficient of unsteady pressure Δp, normalized by $\rho(r_2\omega)^2$
$\Delta C_{p'}$ = coefficient of unsteady pressure $\Delta p'$, normalized by $\rho(r_2\omega)^2$
$\Delta C_{p''}$ = coefficient of unsteady pressure $\Delta p''$, normalized by $\rho(r_2\omega)^2$
F_1, F_2 = lateral fluid force in rotating frame (see Fig. 3)
F_n, F_t = fluid force, normal (n) and tangential (t) to whirl orbit (see Fig. 3)
f_n, f_t = dimensionless fluid force, normal (n) and tangential (t) to whirl orbit, normalized by $\rho\pi r_2^2 b_2\varepsilon\omega^2$
f'_n, f'_t = dimensionless fluid force due to pressure difference across blades: $\Delta p'$, normal (n) and tangential (t) to whirl orbit, normalized by $\rho\pi r_2^2 b_2\varepsilon\omega^2$
f''_n, f''_t = dimensionless fluid force due to pressure distribution on casing wall: $\Delta p''$, normal (n) and tangential (t) to whirl orbit, normalized by $\rho\pi r_2^2 b_2\varepsilon\omega^2$
f = frequency (Hz)
j = imaginary unit
K = dimensionless direct stiffness coefficient, normalized by $\rho\pi r_2^2 b_2\omega^2$
k = dimensionless cross-coupled stiffness coefficient, normalized by $\rho\pi r_2^2 b_2\omega^2$
M = dimensionless direct added mass coefficient, normalized by $\rho\pi r_2^2 b_2$
m = dimensionless cross-coupled mass coefficient, normalized by $\rho\pi r_2^2 b_2$
p = pressure
Δp = unsteady pressure
$\Delta p'$ = peak-to-peak of unsteady pressure on casing wall at blade passing frequency
$\Delta p''$ = amplitude of unsteady pressure on casing wall with whirling frequency
Re = Reynolds number = $u_2 r_2/\nu$ (where $u_2 = r_2\omega$, ν: kinematic viscosity)
r_2 = impeller outlet radius = 149 mm (see Fig. 2)
t = time
Z_i = number of impeller blades = 12
β = circumferential angular difference between pressure taps P4 and P5 = 60 deg
γ = phase difference (deg)
ε = radius of circular whirl orbit = 0.6 mm
θ = circumferential angle
ρ = fluid density
ϕ = flow coefficient = flow rate/$(2\pi r_2^2 b_2\omega)$
ψ = pressure coefficient = $(p - p_{t1})/\rho(r_2\omega)^2$, p_{t1}: total pressure at inlet
Ω = whirling angular velocity
Ω' = angular velocity of pressure pattern
ω = angular velocity of impeller
Ω/ω = whirl speed ratio

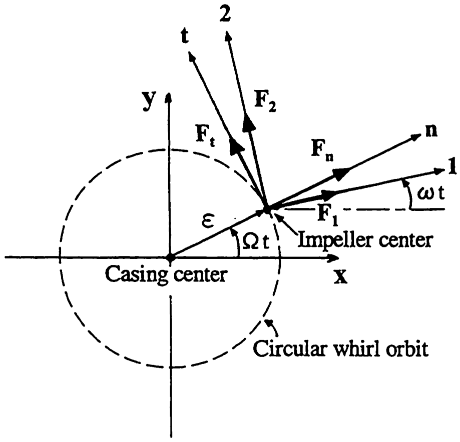

Fig. 3 Scheme showing the rotordynamic forces. F_n and F_t are the normal and tangential component to the whirl orbit. (ε: eccentricity, ω: shaft rotational speed, Ω: whirling speed, (1, 2): rotating frame of the force balance, (*n*, *t*): normal and tangential to the whirl orbit)

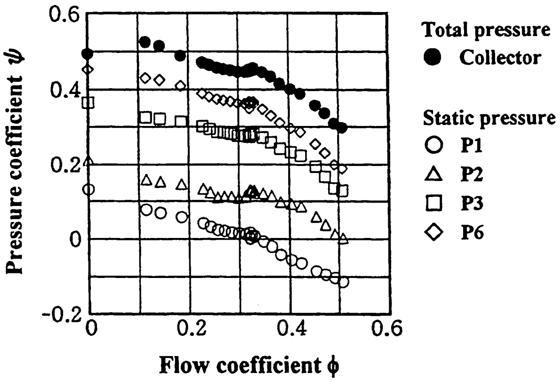

Fig. 4 Pressure performance of the test impeller and steady pressure on the casing wall without eccentricity, pressure coefficient ψ versus flow coefficient ϕ (uncertainty in ψ ± 0.005, in ϕ ± 0.01)

from the inlet to outlet. In the present tests, an eccentricity $\varepsilon = 0.6$ mm was used for the whirl orbit radius. In this condition, the tip clearance varies in the angular direction in the range of 0.4 mm~1.6 mm at the inlet and 0.8 mm~1.2 mm at the outlet in phase respectively, due to the whirling motion.

Instrumentation and Data Acquisition System. The impeller is supported by the main shaft through a rotating force balance with a 4-axis force sensor, as shown in Fig. 1. The force balance is composed of two couples of parallel plates and 4 strain gauges per plate to measure the 4-axis forces (2 forces and 2 force moments). The strain signals were taken out through a slipring. The output signals from the strain gauges are converted to the forces (two) and moments (two) components using a transfer matrix determined from a dynamic calibration test. The outputs start to be recorded at the instant when both the direction of the eccentricity (Ωt) and the impeller rotational angle (ωt) come to a prescribed orientation. Figure 3 shows the situation at time t after the start of data recording, with both of the above directions set to be in x-direction. Output signals were ensemble-averaged over 32 whirl orbits based on the triggering signal that indicates the instant $\Omega t = \omega t = 0$ in Fig.3. The forces measured by the rotating force balance give the lateral components of the fluid force, F_1 and F_2 in a frame rotating with the impeller. The force components normal (F_n) and tangential (F_t) to the whirl orbit, which are useful for the rotor vibration analysis, were obtained from F_1 and F_2 using the angle $(\omega - \Omega) \times t$ between the frame (1, 2) and (n, t), as shown in Fig. 3. Both the fluid forces and force moments on the test impeller were measured in the present study. However in this paper, we focus only on the fluid forces, which play a primary important role for the whirl stability. Measured fluid forces are normalized as $f_n,\ f_t = F_n,\ F_t/(\rho\pi r_2^2 b_2 \varepsilon \omega^2)$, where ρ is fluid density. Uncertainty in the dimensionless fluid forces f_n and f_t is ±1.5. We should note here that the tangential fluid force, f_t, is destabilizing for the whirling motion when $f_t \times (\Omega/\omega) > 0$. (i.e., f_t and Ω/ω are both positive or both negative.) In the case of the normal fluid force, f_n, a positive (outward) force could be considered as a destabilizing force in the sense that it tends to increase the radius of the whirl orbit.

P1~P6 in Fig. 2 show the location of pressure taps to measure the steady and unsteady pressure. P1~P3 and P6 were used to measure the steady pressure with a manometer. P6 is located downstream of the impeller at radius $r = 163$ mm (i.e., $r/r_2 = 1.09$.) In addition to this, P1~P3 and P4, P5 were used to measure the unsteady pressure with pressure transducers. P1~P3 on the casing wall are facing the impeller tip. P4 and P5 are located just upstream (6 mm) of the impeller inlet at different circumferential positions (separation angle, $\beta = 60$ deg.) to facilitate examination of the circumferential propagation of a rotating flow instability (described later). The diameter of the pressure taps, P1~P3, is 1 mm and silicone oil was filled in the cavity in front of the pressure transducers. The pressure transducers at P4 and P5 were installed flush with the casing wall. The resonance frequency of the measurement system is 2.2 kHz, while the blade passing frequency is 80 Hz ($Z_i \times \omega/2\pi$).

Results and Discussions

Compressor Pressure Performance. Figure 4 shows the static pressure coefficient (ψ) and steady pressure on the casing wall at various axial locations plotted against the flow coefficient (ϕ), under the conditions without eccentricity. The design flow coefficient is $\phi_d = 0.424$. From the flow visualization through the transparent casing made of acrylic resin with air bubble injection, backflow onset at the inlet was observed at $\phi = 0.32$, where the pressure rise reaches a local peak. The performance curve has a positive slope in a range of $\phi = 0.30$~0.32. The flow rates less than $\phi = 0.32$ will be called hereafter the low flow rates. For the measurements of fluid forces, the flow rate was varied from $\phi = 0.185$ to $\phi = 0.508$.

Fluid Forces Measured With Force Balance. Figure 5 shows the dimensionless normal, f_n, and tangential, f_t, fluid forces measured directly by the force balance versus the whirl speed ratio, Ω/ω, for various flow rates. From these results, it can be seen that the tangential fluid forces, f_t, on the unshrouded centrifugal impeller are destabilizing at small positive whirl speed ratio in the range $0 < \Omega/\omega < 0.3$ throughout all the flow range, even without the interaction between the impeller and volute casing or vaned diffuser. At the design flow rate of $\phi_d = 0.424$, the normal component is roughly quadratic and the tangential component is linear with whirl speed ratio. This was also found to be true for the case of a shrouded pump impeller in volute casing (Jery et al., 1985). From the quadratic behavior, it is suggested that the added mass effect contributes substantially to the normal component at the design flow rate. The direct added mass (M), cross-coupled added mass (m), direct damping (C), cross-coupled damping (c), direct stiffness (K), and the cross-coupled stiffness (k) can be obtained from rotordynamic force data if force can be expressed as a quadratic function of Ω/ω (Childs (1993) and Brennen (1994)). Table 1 presents the dimensionless rotordynamic coefficients obtained from the fluid forces in Fig. 5 (e) at the design flow rate. The dimensionless direct added mass coefficient, M, is 3.04, and "whirl ratio", k/C, is 0.34. These characteristics are the same as a shrouded pump impeller in volute casing (Jery et al., 1985). The dimensionless direct stiffness coefficient, K, is 1.82 (positive), while it is negative for a shrouded pump impeller. However, it should be noted here that the fluid forces change dramatically at

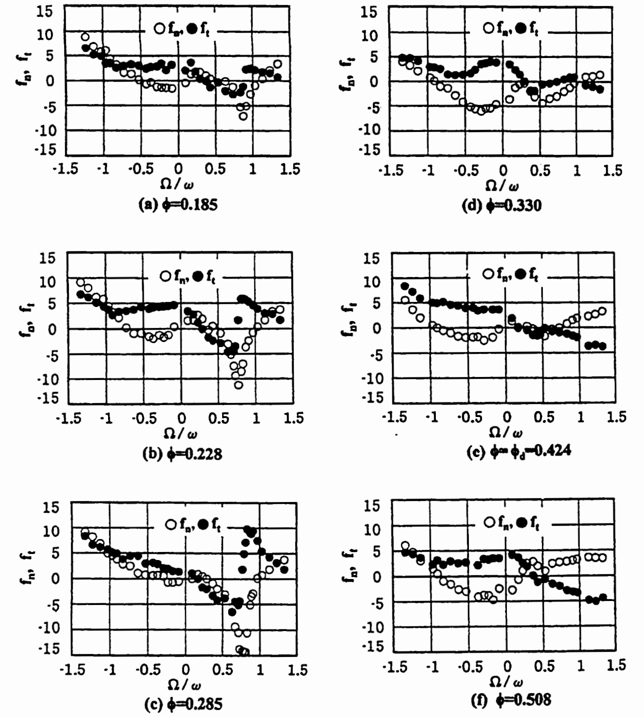

(a) ϕ=0.185 (d) ϕ=0.330 (b) ϕ=0.228 (e) ϕ=ϕ_d=0.424 (c) ϕ=0.285 (f) ϕ=0.508

Fig. 5 Dimensionless fluid forces for ϕ = 0.185, 0.228, 0.285, 0.330, 0.434 (=ϕ_d), and 0.508 ± 0.01, normal f_n and tangential f_t components versus while speed ratio Ω/ω (uncertainty in f_n, f_t ± 1.5, in Ω/ω ± 0.002)

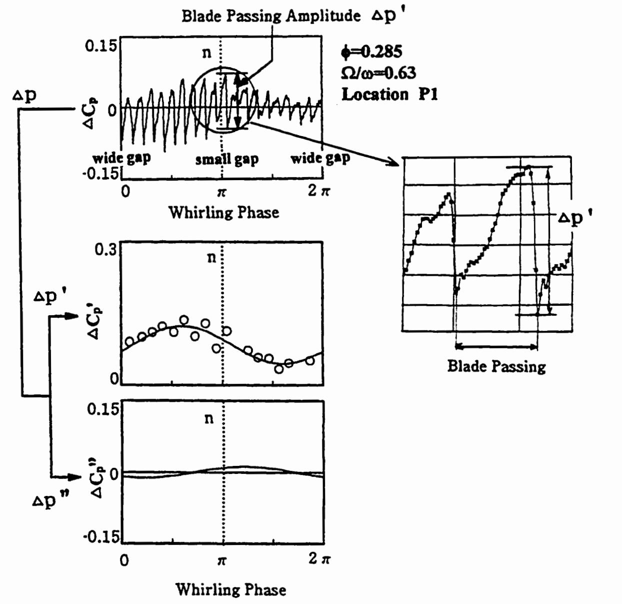

Fig. 6 Evaluation of the peak to peak of the blade passing ($\Delta p'$) and the unsteady pressure with whirling frequency ($\Delta p''$) from the unsteady pressure on the casing wall (Δp), for location of P1, ϕ = 0.285, and Ω/ω = 0.63 (uncertainty in ΔC_p ± 0.005, in ϕ ± 0.01, in Ω/ω ± 0.002)

the low flow rates in the presence of backflow. In particular, at whirl speed ratio close to Ω/ω = 0.8, the tangential component changes significantly from being negative to a high positive value.

Ohashi et al. (1990) reported experimentally that the destabilizing tangential fluid force on a shrouded pump impeller with vaned diffuser increased suddenly at low flow rate for the whirl speed ratio of Ω/ω = 0.05. They attributed this to the rotating stall in the vaned diffuser. Moreover, Tsujimoto et al. (1987) calculated the fluid forces on a whirling impeller in a vaneless diffuser using 2-dimensional vortical flow analysis. They also reported that, at low flow rate, the tangential fluid force becomes destabilizing at the whirl speed ratio (Ω/ω) close to the propagating speed ratio Ω'/ω = 0.157 of the diffuser rotating stall, and Ω'/ω = 0.988 of the impeller rotating stall. Recently, Bently et al. (1998) reported from the experimental results of perturbation test of a centrifugal compressor, that the fluid-induced direct stiffness drops dramatically during rotating stall. The significant change of the fluid forces for Ω/ω = 0.8 in the present study will be discussed later from the detailed examination of the unsteady pressure on the casing wall.

Table 1 Dimensionless rotordynamic coefficients for ϕ_d = 0.424

M, m : normalized by $\rho\pi r_2^2 b_2$
C, c : normalized by $\rho\pi r_2^2 b_2 \omega$
K, k : normalized by $\rho\pi r_2^2 b_2 \omega^2$

M	3.04
m	-0.053
C	4.30
c	-0.081
K	1.82
k	1.48

Force Estimated From Unsteady Pressure Distribution. The fluid forces on the impeller are estimated from the unsteady pressure measurements on the casing wall to possibly obtain a better understanding of their origin. Two simple ways of estimation are employed. The first is to integrate the blade forces that are evaluated from the pressure difference across the blade measured on the casing wall. This corresponds to the nonuniform blade loading model proposed by Thomas (1958) and Alford (1965). The second is simply to integrate the pressure distribution on the casing wall to estimate the reaction forces. In this case the forces due to the pressure distribution and the momentum transfer at the inlet and outlet, and the rate of change of fluid momentum in the impeller are neglected.

Unsteady pressure on the casing wall (Δp at locations P1, P2, and P3) consists of the blade passing frequency and the whirling frequency components. Figure 6 shows a typical example of unsteady pressure, Δp, measured on the casing wall at the location of P1, for ϕ = 0.285, and Ω/ω = 0.63. In this figure, the horizontal axis represents the phase of the whirling during a period, in which the clearance gap is widest at 0, 2π, and smallest at π, at the location of pressure measurement (P1). During one period of the whirling, the number of blades passing by the pressure transducer is $Z_i \times |\omega/\Omega|$. For the condition shown in Fig. 6, nineteen waves ($Z_i \times |\omega/\Omega|$ = 19.05) due to the blade passing are clearly observed. The amplitudes of the component with blade passing frequency, denoted as $\Delta p'$ used for the estimation of the blade loading, were obtained from the reading of peak-to-peak values for each blade passing, as shown in the top of Fig.6. A detail of the pressure wave form of the blade passing is shown in the figure. On the other hand, the pressure fluctuation with whirling frequency, denoted as $\Delta p''$ used for the casing pressure force evaluation, was obtained from the Fourier transform analysis of Δp, as shown in the bottom of Fig. 6.

For the blade load evaluation, it is assumed that $\Delta p'$ shows the pressure difference across the blade at the tip, and the pressure differences from the tip to hub are proportional to the square of its radius. The forces (f_n', f_t') are estimated by integrating the assumed pressure differences on the three segments of the blade using $\Delta p'$

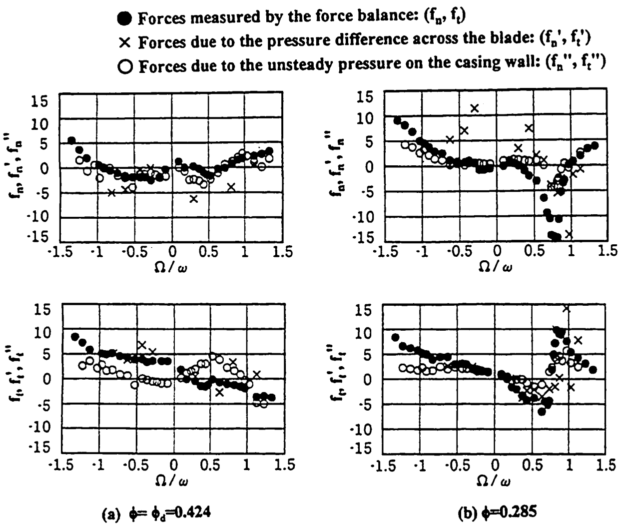

(a) $\phi = \phi_d = 0.424$ (b) $\phi = 0.285$

Fig. 7 Comparisons of the dimensionless direct fluid forces (f_n, f_t) with the estimated fluid forces (f'_n, f'_t) due to the pressure difference across the blade, and (f''_n, f''_t) due to the unsteady pressure on the casing wall (uncertainty in f_n, f_t ± 1.5, in Ω/ω ± 0.002)

at P1, P2, and P3 in consideration of the back swept blade. For the casing pressure force evaluation, the fluid forces (f''_n, f''_t) are obtained by integrating the pressure distributions $\Delta p''$ from the blade leading edge to trailing edge on the casing wall. The pressure distributions are interpolated and extrapolated from $\Delta p''$ at P1, P2, and P3.

Figure 7 shows the comparison of the direct fluid forces (f_n, f_t) measured with the force balance and the estimated forces (f'_n, f'_t), and (f''_n, f''_t), for the design ($\phi_d = 0.424$) and low flow rate ($\phi = 0.285$) conditions. The fluid forces (f''_n, f''_t) agree fairly well with (f_n, f_t), while (f'_n, f'_t) are not in good agreement. Thomas (1958) and Alford (1965) explained the destabilizing mechanism in axial flow turbines from the blade loading nonuniformity due to the change in tip clearance. The present results may suggest that some fraction of the fluid force on the impeller is caused by the nonuniform pressure distribution on the casing wall, so that a different flow model is needed to explain the rotordynamic forces on unshrouded centrifugal impellers.

Coupling of Whirling Motion With Rotating Flow Instability at Low Flow Rate. Figures 8 and 9 show the unsteady pressure at the inlet at the design ($\phi_d = 0.424$) and lower flow rate ($\phi = 0.285$) conditions, without eccentricity. Figures 8 (*a*) and 9 (*a*) show the wave forms measured at the locations of P4 and P5; P4 and P5 are at the same axial location, but P5 is 60 deg ahead of P4 in the direction of the impeller rotation. Figures 8 (*b*) and 9 (*b*) show the time averaged cross spectra between P4 and P5, and Figs. 8 (*c*) and 9 (*c*) the phase (γ) of the pressure at P5 relative to that at P4. At the design flow rate, the blade passing ($f = 80$ Hz ($Z_i \times \omega/2\pi$)) is clearly shown in the wave form. However, it is not very clear at the lower flow rate. At the low flow rate, there are some peaks in the cross spectrum (Fig. 9(*b*)), although the cross of amplitudes ($\Delta p_4 \times \Delta p_5$) of these peaks are much smaller (approximately 1~3%) than that of the blade passing frequency. The discrete components (i), (ii), and (iii), in Figs. 9 (*b*) and (*c*), have the frequency of $f = 5.3$, 10.8, and 17.0 Hz, and the phase $\gamma = -60$, -150, and -200 deg, respectively. These values of phase difference are close to integer multiples of circumferential angular distance ($\beta = 60$ deg) of two sensors; i.e., $\gamma \cong -n\beta$, $n = 1, 2$, and 3. This suggests that pressure patterns with the number of cells $n = 1$, 2, and 3 are rotating at the inlet much like conventional rotating stall. However, unlike conventional rotating stall, these frequency components (i), (ii) and (iii) are found only at the inlet. The propagating speed ratio of these components is $\Omega'/\omega = f/n(\omega/2\pi) \approx 0.79$ which is very close to the value of $\Omega/\omega = 0.8$ where the abrupt change in f_n and f_t is found at the low flow rate under whirling motion. The group of frequency components (iv) distributed over a wide range of frequency $f = 20\sim60$ Hz has the characteristic that the phase (γ) decreases linearly with the increasing frequency f. Here, when we assume a circumferentially propagating pressure pattern Δp with frequency f and propagating speed Ω', that is $\Delta p \propto \exp\{2\pi f j \times (t - \theta/\Omega')\}$, the phase γ measured between P4 and P5 is expressed as $\gamma = -2\pi f\beta/\Omega'$ (where $\theta = \beta = 60$ deg). With constant Ω', this relation between γ and f is linear. This situation agrees with the component (iv) found in the range of $f = 20\sim60$ Hz as shown in Fig. 9 (*c*). From the slope of $\Delta\gamma/\Delta f$ in Fig. 9 (*c*), the propagating speed ratio was estimated to be $\Omega'/\omega = 0.43$ in the present study. From the above discussion, frequency components (i)~(iii) correspond to discrete frequencies where $2\pi f/\Omega' = n = 1$, 2, and 3 (where $\Omega'/\omega = 0.79$), while for the frequency component range (iv) the value of $2\pi f/\Omega'$ varies continuously from 7 to 21 as f varies from 20~60 Hz ($\Omega'/\omega = 0.43$). All of the components (i)~(iv) appeared at lower flow rate $\phi < 0.32$ where the inlet backflow was observed from the flow visualization. However, further study is needed to clarify the relation between the backflow and these pressure fluctuations.

Kameier et al. (1997) also observed similar rotating pressure pattern with a constant slope $\Delta\gamma/\Delta f$ at low flow rate in an axial compressor. In this case, the propagating speed ratio increased

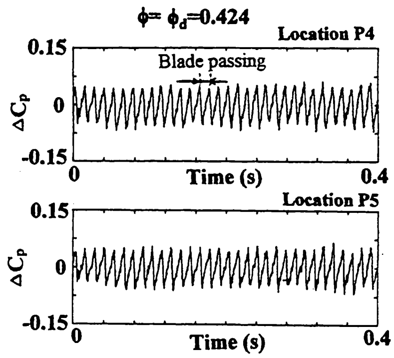

(a) Wave form

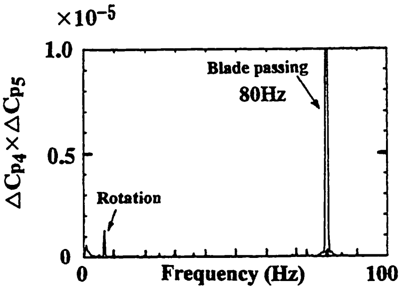

(b) Cross spectrum

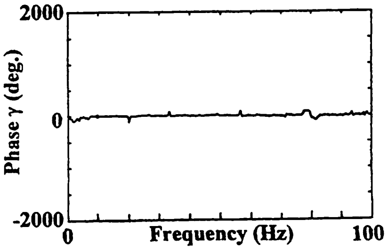

(c) Phase spectrum

Fig. 8 Typical wave form of unsteady pressure, cross, and phase spectrum at the impeller upstream locations P4 and P5, $\phi = \phi_d = 0.424 \pm 0.01$, without eccentricity (uncertainty in ΔC_p ± 0.005, in frequency f ± 0.4 Hz, in phase γ ± 5 deg)

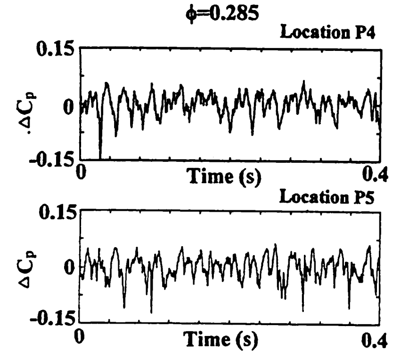

(a) Wave form

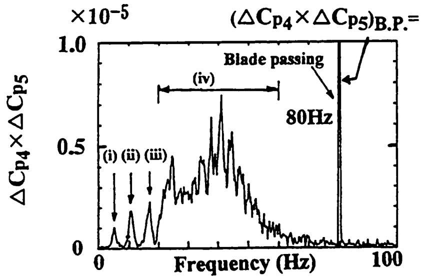

(b) Cross spectrum

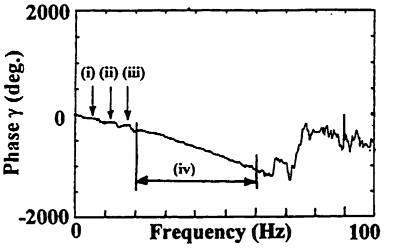

(c) Phase spectrum

Fig. 9 Typical wave form of unsteady pressure, cross, and phase spectrum at the impeller upstream locations P4 and P5, $\phi = 0.285 \pm 0.01$, without eccentricity (uncertainty in $\Delta C_p \pm 0.005$, in frequency $f \pm 0.4$ Hz, in phase $\gamma \pm 5$ deg)

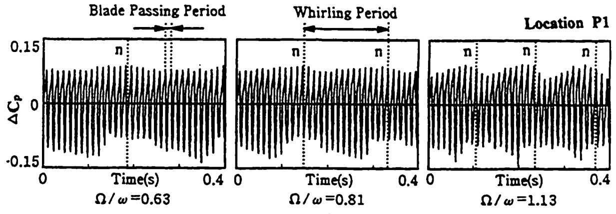

(a) $\phi = \phi_d = 0.424$

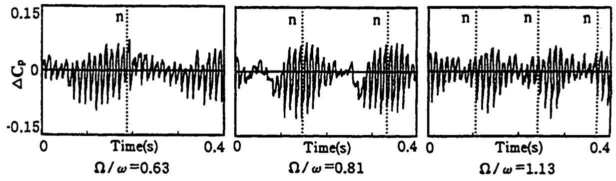

(b) $\phi = 0.285$

Fig. 10 Comparison of the pressure fluctuations on the casing wall between $\phi = \phi_d = 0.424$ and $\phi = 0.285$ with whirling motion $\varepsilon = 0.6$ mm, at location P1 for $\Omega/\omega = 0.63, 0.81, 1.13$ (uncertainty in $\Delta C_p \pm 0.005$, in $\Omega/\omega \pm 0.002$, in $\phi \pm 0.01$)

from 0.3 to 0.55 as the flow rate decreased. From their experimental results for the cases with two tip clearances (wide and small) and a test with Velcro tape inserted in the tip clearance, they concluded that these patterns of pressure fluctuation are associated with the leakage flow through the tip clearance under reversed flow condition.

Figure 10 shows the comparison of the pressure fluctuations measured at the location P1 with a whirl eccentricity, $\varepsilon = 0.6$ mm. The wave forms of pressure fluctuation were ensemble-averaged 32 times based on the triggering signal that indicates the instant when the direction of the eccentricity and the impeller rotation angle are at a prescribed orientation relative to the pressure transducer. The dotted line, denoted as "n" in the figures, indicates the instant when the smallest tip clearance passes by the pressure transducer. The amplitude of the blade passing component, or the blade loading, varies with the whirling. At the design flow rate (Fig. 10 (*a*)), the variation of the blade loading is not strongly affected by the whirl speed ratio within $\Omega/\omega = 0.63\sim1.13$. However at low flow rate (Fig. 10 (*b*)), the blade loading changes significantly with the whirling motion, and the location of the maximum blade loading (corresponding to the highest peak-to-peak fluctuation) relative to the location of the minimum tip clearance (n) shifts with the change in Ω/ω. The difference of the blade loading is largest at $\Omega/\omega = 0.81$. This and the large change of the fluid forces near $\Omega/\omega = 0.8$ at low flow rates may be caused by the coupling of the whirling motion with the rotating pressure pattern, i.e., component (i), found at the impeller inlet (Figs. 9(*b*) and 9(*c*)).

Conclusions

From the experimental results and discussions, the following conclusions can be drawn:

1. For an open-type centrifugal compressor impeller, the tangential fluid forces become destabilizing at small positive whirl speed ratio ($0 < \Omega/\omega < 0.3$) throughout all the flow range even without the interaction with a volute or vaned diffuser.
2. The forces estimated from the unsteady pressure on the casing wall agree well with the forces measured directly by the force balance. However, the forces estimated from the pressure difference across the impeller blades are not in good agreement with the direct force measurements.
3. The fluid forces change dramatically near the whirl speed ratio $\Omega/\omega = 0.8$ at the low flow rates. As a result, the tangential fluid force has a large positive value and enhances whirling close to this whirl speed ratio..
4. When the rotor has no eccentricity, it was found that pressure patterns with 1, 2 and 3 cells rotate at the impeller inlet with the speed ratio of $\Omega'/\omega = 0.79$ at low flow rates. In addition to this, it was found that the pressure patterns without definite number of cells propagate with the speed ratio of $\Omega'/\omega = 0.43$.
5. From the pressure measurements just downstream of the blade leading edge in presence of whirling motion, it is suggested that the destabilizing fluid force around $\Omega/\omega = 0.80$ is caused by the strong interaction of the whirling motion with the rotating flow pattern with $\Omega'/\omega = 0.79$.

Acknowledgments

The authors wish to express their gratitude for the effort of Mr. Shin Ishizaki in establishing the experimental procedure as a graduate project at Osaka University. They are also deeply grateful to Dr. Bruno Schiavello of Ingersoll-Dresser Pump Company for his extremely helpful and useful comments. The present study was partly supported by the Ministry of Education, Science, Sports and Culture through the Grant-in Aid for Developmental Scientific Research (No.06555055).

References

Adkins, D. R., and Brennen, C. E., 1988, "Analyses of Hydraulic Radial Forces on Centrifugal Pump Impeller," ASME JOURNAL OF FLUIDS ENGINEERING, Vol. 110, pp. 20–28.

Alford, J. S., 1965, "Protecting Turbomachinary from Self-Excited Rotor Whirl," ASME *Journal of Engineering for Power*, Vol. 87, pp. 334–344.

Bently, D. E., and Goldman, P., 1998, "Destabilizing Effect of Aerodynamic Forces in Centrifugal Compressors," *Proceedings of the 7th International Symposium on Transport Phenomena and Dynamics of Rotating Machinery*, Honolulu, Hawaii, Vol. A, pp. 306–315.

Bolleter, U., Wyss, A., Whelte, I., and Sturchler, R., 1987, "Measurement of Hydraulic Interaction Matrices of Boiler Feed Pump Impeller," ASME *Journal of Vibration, Acoustics, Stress and Reliability in Design*, Vol. 109, pp. 144–151.

Brennen, C. E., 1994, *Hydrodynamics of Pumps*, Concept ETI, and Oxford University Press.

Childs, D. W., 1989, "Fluid Structure Interaction Forces at Pump-Impeller-Shroud Surfaces for Rotordynamic Calculation," ASME *Journal of Vibration, Acoustics, Stress and Reliability in Design*, Vol. 109, pp. 144–151.

Childs, D. W., 1993, *Turbomachinery Rotordynamics*, Wiley, New York.

Colding-Jorgensen, J., 1992, "Prediction of Rotor Dynamic Destabilizing Forces in Axial Flow Compressor," ASME Journal of Fluids Engineering, Vol. 114, pp. 621–625.

Ehrich, F., 1993, "Rotor Whirl Forces Induced by the Tip Clearance Effect in Axial Flow Compressor," ASME *Journal of Vibration and Acoustics*, Vol. 115, pp. 509–515.

Guinzburg, A., Brennen, C. E., Acosta, A. J., and Caughy, T. K., 1994, "Experimental Results for the Rotordynamic Characteristics of Leakage Flow in Centrifugal Pump," ASME Journal of Fluids Engineering, Vol. 116, pp. 110–115.

Jery, B., Acosta, A. J., Brennen, C. E., and Caughy, T. K., 1985, "Forces on Centrifugal Pump Impellers," *Proceedings of the 2nd International Pump Symposium*, Houston, Texas, pp. 21–32.

Kameier, F., and Neise, W., 1997, "Experimental Study of Tip Clearance Losses and Noise in Axial Turbomachines and Their Reduction," ASME *Journal of Turbomachinery*, Vol. 119, pp. 460–471.

Martinez-Sanchez, M., Jaroux, B., Song, S. J., and Yoo, S., 1995, "Measurement of Turbine Blade-Tip Rotordynamic Excitation Forces", ASME *Journal of Turbomachinery*, Vol. 117, pp. 384–392.

Ohashi, H., Sakurai, A., and Nishihama, J., 1988, "Influence of Impeller and Diffuser Geometries on the Lateral Fluid Forces of Whirling Centrifugal Impeller," NASA CP. 3026, pp. 285–306.

Ohashi, H., Imai, H., Sakurai, A., and Nishihama, J., 1990, "Lateral fluid Forces of Whirling Centrifugal Impellers with Various Geometries," *The 3rd Japan-China Joint Conference of Fluid Machinery*, Vol. II, pp. 147–153.

Ohashi, H., Imai, H., and Tsuchihashi, T., 1991, "Fluid Force and Moment on Centrifugal Impeller in Precession Motion," ASME *Fluid Machinery Forum*, FED-Vol. 119, pp. 57–60.

Song, S. J., and Martinez-Sanchez, M., 1997, "Rotordynamic Forces Due to Turbine Tip Leakage: Part 1 - Blade Scale Effects, Part II - Radius Scale Effects and Experimental Verification," ASME *Journal of Turbomachinery*, Vol. 119, pp. 605–703, and pp. 704–713.

Thomas, H. J., 1958, "Instabile Eigenschwingungen von Turbinenlaeufern Angefacht durch die Spaltstroemung in Stopfubuchsen und Bechauchflug (Unstable Nature Vibrations of Turbine Rotors Induced by the Clearance Flows in Glands and Blading)," *Bulletin de L.A.I.M.*, Vol. 71, No.11/12, pp. 1039–1063.

Tsujimoto, Y., Acosta, A. J., 1987, "Theoretical Study of Impeller and/or Vaneless Diffuser Attributed Rotating Stall and Their Effects on Whirling Instability of Centrifugal Impeller," Work Group on the Behavior of Hydraulic Machinery under Steady Oscillatory Conditions, Lille, France.

Tsujimoto, Y., Acosta, A. J., and Brennen C. E., 1988a, "Theoretical Study of Fluid Forces on Centrifugal Pump Impeller Rotating and Whirling in a Volute," ASME *Journal of Vibration, Acoustics, Stress and Reliability in Design*, Vol. 110, pp. 263–269.

Tsujimoto, Y., Acosta, A. J., and Yoshida, Y., 1988b, "A Theoretical Study of Fluid Forces on Centrifugal Pump Impeller Rotating and Whirling in a Vaned Diffuser," NASA CP. 3026, pp. 307–322.